INSTITUTE OF PHYSICS PUBLISHING JOURNAL OF PHYSICS: CONDENSED MATTER

J. Phys.: Condens. Matter **14** (2002) 12287–12300 PII: S0953-8984(02)40032-X

Phase transition in lead titanate thin films: a Brillouin study

P Kuzel[1], C Dugautier[2], P Moch[2], F Le Marrec[3] and M G Karkut[3]

[1] Institute of Physics, Academy of Sciences of the Czech Republic, Na Slovance 2, 18221 Prague 8, Czech Republic
[2] Laboratoire des Propriétés Mécaniques et Thermodynamiques des Matériaux, CNRS, Université Paris-Nord, Av. J-B Clément, 93430 Villetaneuse, France
[3] Laboratoire de Physique de la Matière Condensée, Université de Picardie Jules Verne, 80039 Amiens, France

Received 29 July 2002
Published 15 November 2002
Online at stacks.iop.org/JPhysCM/14/12287

Abstract

The elastic properties of both polycrystalline and epitaxial $PbTiO_3$ (PTO) thin films are studied using Brillouin scattering spectroscopy. The epitaxial PTO films were prepared by pulsed laser ablation on (1) a [0 0 1] single crystal of $SrTiO_3$ (STO) doped with Nb and (2) a [0 0 1] STO buffered with a layer of $YBa_2Cu_3O_7$. The polycrystalline PTO films were prepared by sol–gel on a Si substrate buffered with TiO_2 and Pt layers. The data analysis takes into account the ripple and the elasto-optic contributions. The latter significantly affects the measured spectra since it gives rise to a Love mode in the p–s scattering geometry. At room temperature, the spectra of the epitaxially grown samples are interpreted using previously published elastic constants of PTO single crystals. Sol–gel samples exhibit appreciable softening of the effective elastic properties compared to PTO single crystals: this result is explained by taking into account the random orientation of the microscopic PTO grains. For both the polycrystalline and the epitaxial films we have determined that the piezoelectric terms do not contribute to the spectra. The temperature dependence of the spectra shows strong anomalies of the elastic properties near the ferroelectric phase transition. Compared to the bulk, T_C is higher in the sol–gel films, while in the epitaxial films the sign of the T_C shift depends on the underlying material.

1. Introduction

The study of ferroelectric thin films is the subject of increasingly intense interest due to both the technological promise of these materials and to the intrinsic interest generated by the ability to form epitaxial thin and ultra-thin films and heterostructures. A number of applications involving thin ferroelectric films have been proposed and some of them are now

being developed in the field of memories, of microactuators and of devices using surface acoustic waves. They take advantage of the high dielectric constants, of the spontaneous polarization and of the large piezo-electric coefficients of these complex oxide materials. It has been suggested theoretically [1] and there have been experimental observations [2] that ferroelectricity does not necessarily vanish for small thicknesses and can even exist in films consisting in a stack of a few atomic planes. However, the observed properties do in fact depend on the conditions of growth and on the underlying substrates, buffer and electrode layers. The sol–gel technique, popular because of its ability to generate films quickly and inexpensively, generally leads to polycrystalline orientation. With pulsed laser deposition (PLD) it is often possible to grow high quality epitaxial films on single-crystal substrates and buffer layers. The detailed characteristics are very sensitive to the geometrical, chemical and electrical properties of these substrates. The presence of two-and three-dimensional stresses in the films, at least partly related to the mismatch of the lattice parameter between the substrate and the film [3–7], can induce large shifts of the ferroelectric–paraelectric phase transition. Thus the study of the elastic properties of ferroelectric thin films is expected to provide a key for a better understanding of the role of the substrates, of the interfaces and of the thicknesses on the physical behaviour of the ferroelectric structures. We have chosen to focus on the compound $PbTiO_3$ (PTO), since the properties of the single PTO crystals have given rise to a number of experimental studies (see for example [8–10]), thus allowing a detailed comparison with the properties of the films.

This work was achieved using Brillouin scattering spectroscopy: this technique is a powerful tool in the investigation of elastic properties but the analysis of the experimental spectra related to the propagating hypersonic surface waves in layered structures is rather complex [11–17]. Hence we will first provide some background on Brillouin scattering in layered structures before proceeding to the rest of the study. In the following sections we give a brief description of the measured samples and of the experimental set-up. Then we present and discuss the comparative results obtained at room temperature in the randomly oriented sol–gel PTO films and in the epitaxial laser ablated PTO films. Finally, the last section is devoted to the temperature dependence of the Brillouin spectra and to their connection with the ferroelectric–paraelectric phase transition.

2. Description of Brillouin scattering in layered structures

2.1. Acoustic waves in layered structures

The theory of the propagation of acoustic waves in stacked structures including the piezoelectric effects has been treated by Farnell [18]. We assume that the normal to the layers is parallel to the x_3-axis and we illustrate the experimental geometry in figure 1. The propagating eigenmodes, harmonic waves of wavevector $\boldsymbol{q}_\parallel$ (see figure 1), are described by Christoffel's equation together with Poisson's equation for the three displacement components u_1, u_2 and u_3 and for the electrostatic potential φ:

$$\begin{aligned} \rho\Omega^2 u_i &= C^E_{ijkl}\frac{\partial u_l}{\partial x_j \partial x_k} + e_{jki}\frac{\partial \varphi}{\partial x_j \partial x_k} \\ 0 &= e_{ijk}\frac{\partial u_k}{\partial x_i \partial x_j} + \varepsilon^S_{ij}\frac{\partial \varphi}{\partial x_i \partial x_j} \end{aligned} \tag{1}$$

where ρ is the density, C^E_{ijkl} is the elastic tensor at constant electric field, e_{ijk} is the piezoelectric stress tensor, ε^S_{ij} is the dielectric permittivity tensor at constant strain and Ω is the angular frequency of the acoustic wave.

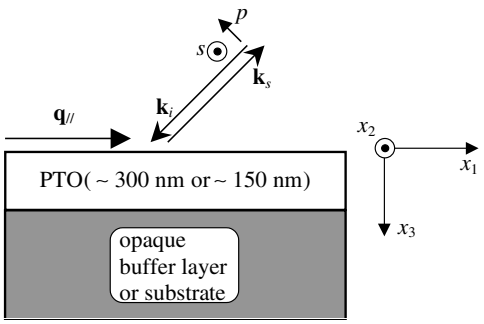

Figure 1. Schematic diagram of the scattering geometry.

Introducing a frequency-dependent 4×4 matrix operator Γ_{il} these equations of motion can be formally written as $\Gamma_{il}u_l = 0$ (with $i, l = 1$–4), where the potential φ is denoted as u_4. These equations are solved for each layer in the stack and for the substrate. Writing down the suitable boundary conditions [18] allows us to find the eigenfrequencies of the modes and to calculate the corresponding distribution of the displacement field and of the electrostatic potential.

In layered structures, the incident radiation is usually scattered by acoustic phonons via two physically distinct processes: (i) the surface or interface ripple and (ii) the bulk elasto-optic coupling. The spectra generally consist of a pseudo-Rayleigh surface mode and of a set of guided modes within the thin film structure. All these modes are analysed in terms of displacement correlation functions. Using the fluctuation–dissipation theorem, these correlation functions can be calculated from a susceptibility tensor G_{ij} which satisfies the above equations of motion when a Dirac δ-function source term is added to the right-hand side:

$$\Gamma_{il}G_{lk}(\Omega, \boldsymbol{q}_{\parallel}, x_3, x_3') = I_{ik}\delta(x_3 - x_3') \tag{2}$$

where I_{ik} is a unit tensor.

2.2. *Light scattering by ripple*

The scattered radiation arising from the ripple is related to the autocorrelation function g_{33} of the displacement component normal to the surface (denoted as u_3). If the upper layer of the stack is opaque then g_{33} will consist only of the contribution from the top surface (the air–thin film interface). The light intensity scattered by the ripple is then proportional to

$$g_{33} \equiv \langle u_3(x_3 = 0)u_3^*(x_3' = 0)\rangle = \frac{kT}{\hbar\Omega}\mathrm{Im}\{G_{33}(\Omega, \boldsymbol{q}_{\parallel}, x_3 = 0, x_3' = 0)\}, \tag{3}$$

where the symbol $\langle\cdots\rangle$ stands for the statistical mean value. If, on the other hand, the upper layer is transparent, interference effects of the ripple scattering contributions from several interfaces occur and these effects are accounted for by an appropriate linear combination of the $G_{33}(\Omega, \boldsymbol{q}_{\parallel}, x_3 = h_i, x_3' = h_j)$ where h_i and h_j denote the x_3-coordinates of i and j interfaces. The amplitudes of the coefficients of this linear combination depend on the ripple scattering cross-section [12, 14] and their phases depend on the optical paths. These coefficients are calculated from the continuity conditions of the optical electromagnetic field on the undulating interfaces. In this article, since all experiments were performed with samples having a transparent PTO top layer deposited on an opaque layer, we will be concerned with two contributions only: those from the upper and from the lower surfaces of the PTO thin film.

2.3. Light scattering through elasto-optic coupling

The above mentioned ripple process is usually dominant for opaque materials. However, in transparent media the elasto-optic contribution can be large, and this is in fact what we observe in our spectra described in the next sections. The corresponding scattered field is related to the strain-induced electric polarization by

$$P_i = -\varepsilon_{ik}\varepsilon_{jl}\, p_{klmn}\, u_{mn} E_j, \tag{4}$$

where p_{klmn} is the photo-elastic tensor, ε_{ik} is the dielectric tensor and $u_{mn} = \partial u_m/\partial x_n$ is a displacement gradient term (strain). The scattered radiation is then related to a linear combination of the correlation functions of the displacement derivatives $\langle u_{mn}(x_3)u_{kl}(x_3')\rangle$ integrated over the entire sample. The terms of this linear combination are weighted by the photo-elastic coefficients. Due to the large optical absorption of the substrates and of the buffer layers used in our samples (see the next section) the integration can be restricted to the PTO film. In most crystals the $p_{\lambda\mu}$ coefficients with $\lambda \leqslant 3$, $\mu \leqslant 3$ (in Voigt notation) largely dominate. Careful examination of the expression providing the elasto-optic scattered intensity in the p–p polarization geometry then allows us to conclude that the leading terms are proportional to (in the slowly varying envelope approximation for the scattered field)

$$g_{jk} = \frac{kT}{\hbar\Omega}\mathrm{Im}\left\{\int_0^h \mathrm{d}x_3' \int_0^h \mathrm{d}x_3\, E_i(x_3)E_i^*(x_3')\frac{\partial^2 G_{jk}(\Omega, \boldsymbol{q}_\parallel, x_3, x_3')}{\partial x_j \partial x_k'}\exp(\mathrm{i}k_\perp(x_3' - x_3))\right\} \tag{5}$$

where h is the PTO layer thickness, i, j and k can take the values 1 or 3 and $k_\perp$ is the normal component of the optical wavevector inside the film. The evaluation of g_{11} can often provide a semi-quantitative evaluation of the expected inelastic scattered intensity [19], namely that of its high frequency part, which is referred to as the longitudinal resonance in the case of a semi-infinite medium [20].

Exceptionally, in some structures, shear guided modes can be detected in the p–s polarization geometry [14]: these are the so-called Love modes. They contribute to the scattered spectra through elasto-optic coupling and are related to the photoelastic coefficients $p_{\lambda\lambda}$, where $\lambda = 4, 6$. Their frequencies are accounted for by the susceptibility G_{22}:

$$g_{22} = \frac{kT}{\hbar\Omega}\mathrm{Im}\left\{\int_0^h \mathrm{d}x_3' \int_0^h \mathrm{d}x_3\, E_j(x_3)E_k^*(x_3')\frac{\partial^2 G_{22}(\Omega, \boldsymbol{q}_\parallel, x_3, x_3')}{\partial x_j \partial x_k}\exp(\mathrm{i}k_\perp(x_3' - x_3))\right\}, \tag{6}$$

with $j, k = 1, 3$. In the following discussions we will use the above approximations and we will interpret the measured spectra using the above defined correlation functions g_{jk}.

3. PTO thin films: preparation and characterization

Two types of sample were studied: polycrystalline and epitaxial.

The polycrystalline PTO films were produced by the sol–gel method. These films were grown by Malic at the Stefan Institute of Ljubiana (Slovenia) on a Si/TiO_2(250 nm)/Pt(250 nm) substrate. X-ray diffraction spectra, obtained after thermal annealing of the films, showed a nearly random crystalline orientation and a noticeable reduction of the tetragonal c/a ratio compared to its value in the bulk crystal (1.045 instead of 1.066). The film thicknesses were measured by scanning electron microscopy (SEM): the typical values of the PTO layers were found to be around 300 nm.

The epitaxial films were deposited by laser ablation. The first one was prepared on a Nb-doped $SrTiO_3$[0 0 1] single-crystal substrate maintained at 650 °C in a partial oxygen pressure of 2 mbar. Reflection high energy electron diffraction (RHEED) produced sharp well defined streaks which were aligned with the streaks produced by the STO substrate. This indicates that

the PTO surface is smooth and that the film is epitaxially oriented with respect to the substrate. X-ray diffraction spectra showed only (0 0 1) reflections which indicate that the film is *c*-axis oriented (*c* domains) with a c/a ratio of approximately 1.06. The measured thicknesses were about 150 nm. In order to study the influence of the substrate upon the ferroelectric–paraelectric phase transition, we also prepared samples with an intermediate 250 nm $YBa_2Cu_3O_7$ (YBCO) buffer layer. At room temperature YBCO is orthorhombic with a *c* axis of 1.167 nm and the *a* and *b* parameters of 0.382 and 0.388 nm respectively. These values are fairly close to those of the STO substrate ($a = 0.3905$ nm) and the *a* axis of bulk PTO ($a = 0.3899$ nm). We observed RHEED streaks both for the YBCO buffer layer and for the PTO film, again indicating fairly smooth surfaces and epitaxial orientation. We point out that the RHEED images were of higher quality for the PTO/STO sample, thus indicating superior structural quality for this film. X-ray diffractometry produced only (0 0 1) reflections for both YBCO and PTO again indicating *c*-axis films [21].

Finally, the films were imaged using the atomic force microscopy technique: the linear dimensions of the PTO grains in sol–gel samples show a non-negligible dispersion but most of them lie in the 100–150 nm range. The grains are slightly larger in epitaxial films: about 200 nm in the PTO/YBCO/STO sample and about 250 nm in the PTO/STO one.

The samples used for Brillouin scattering experiments were not subjected to any additional poling process such as, for instance, an applied electric field.

4. Experimental set-up

The Brillouin polarized spectra were obtained in a backscattering geometry using a previously described [17] 2 × 3-pass Fabry–Pérot tandem spectrometer. The angle of incidence θ could be varied from 30° to 65°, thus allowing us to scan the amplitude of the wavevector of the observed modes: for a surface mode, the amplitude of the wavevector $\boldsymbol{q}_\parallel$ is $q_\parallel = 4\pi \sin(\theta)/\lambda$, and for a bulk mode the wavevector amplitude is given by $q = 2\pi n/\lambda$ ($\lambda = 514$ nm is the incident radiation wavelength and *n* is the refractive index of the medium). The sample could be rotated about the direction normal to the layers, permitting us to measure the in-plane anisotropy of the surface modes. The scattering geometry is depicted in figure 1. Spectra were taken at temperatures ranging from about 20 up to 575 °C produced by a furnace constructed in house.

5. Room-temperature measurements: results and discussion

5.1. Sol–gel films

The recorded scattered spectral density arises both from the usual ripple mechanism, and from the elasto-optic contribution. The latter is found to be rather large: it is due to the negligible optical absorption of the PTO films and, presumably, to the large values of some of the elasto-optic coefficients $p_{\lambda\mu}$. A convincing argument in favour of a significant bulk contribution is the intense p–s Brillouin spectrum. It is well known that ripple scattering vanishes in the cross-polarized scattering geometry. Consequently, the observed spectrum is the result of an elasto-optic process and allows us to evidence a Love mode. Typical experimental spectra, including this last feature, are displayed in figure 2: they are compared with the calculated ones using the fitted elastic constants listed in table 1. The fits represent the calculated cumulative contribution of ripple and elasto-optic processes. In figure 3, we show the experimental and calculated variations of the surface velocities ($\Omega/q_\parallel$) versus $q_\parallel h$. As expected from the previously mentioned random grain orientation of the sol–gel produced films, the experimental spectra do not show in-plane anisotropy.

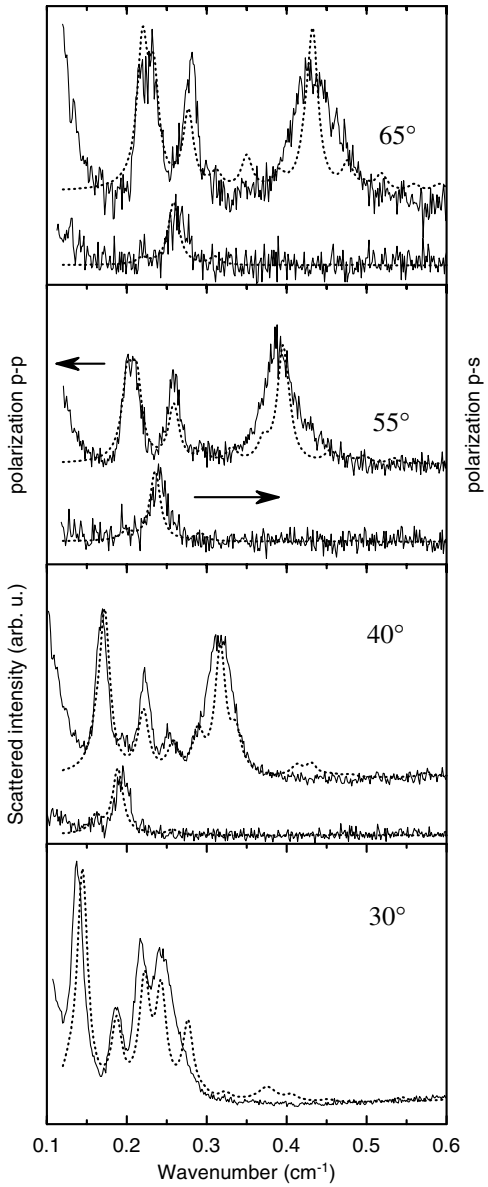

Figure 2. Sol–gel sample spectra recorded at several angles of incidence: full curves. Calculated spectra: dotted curves.

To interpret the experimental results, the mechanical properties of the Si substrate and of the underlying TiO_2 and Pt buffer layers were needed. For the Si and the TiO_2 sublayer, we used literature values of the elastic constants since moderate variations of these constants will not significantly affect the Brillouin spectra. In contrast, the measured spectra do depend upon the parameters characterizing the opaque Pt film adjacent to the PTO layer. Consequently, we investigated a Pt thin film by Brillouin scattering and we were able to fit the spectra assuming an isotropic medium with $C_{11} = 370$ GPa and $C_{44} = 65$ GPa. These experimentally fitted

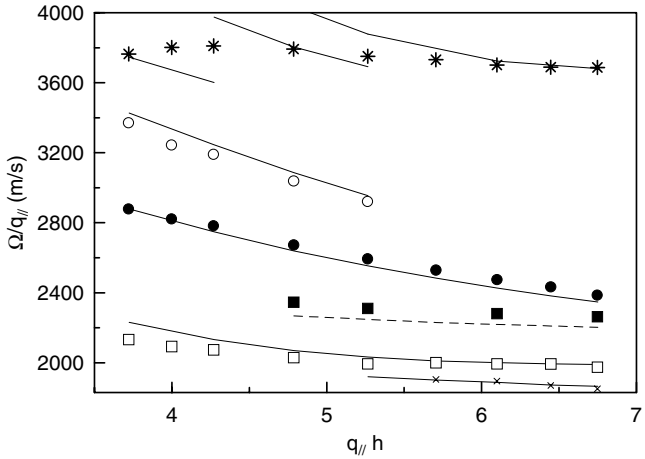

Figure 3. Sol–gel sample: variation of surface velocities ($\Omega/q_\parallel$) versus $q_\parallel h$ (h is the thickness of the PTO film). Experimental points in p–p polarization: (×) guided mode within the Pt layer; (□) Rayleigh surface mode; (●, ○) guided modes within the PTO/Pt bilayer; (∗) longitudinal resonance. In p–s polarization: (■) Love mode. Calculations: (solid curves) p–p polarization; (dashed curve) p–s polarization.

Table 1. Room-temperature elastic constants at constant electric field (C_{ij}) and temperatures of the ferroelectric phase transition (T_C) in PTO films compared to the values (in italics) derived from single-crystal data [11]. The derivation of C_{12} and C_{66} from in-plane anisotropy results needs additional further experimental confirmation.

	C_{44} (=C_{55}) (GPa)	C_{11} (=C_{22}) (GPa)	C_{33} (GPa)	C_{13} (=C_{23}) (GPa)	C_{66} (GPa)	C_{12} (GPa)	T_C (°C)
Bulk crystal	*69*	*237*	*60*	*70*	*104*	*90*	*490*
STO/PTO (epitaxial)	69	237	60	70	135 (?)	120 (?)	530
STO/YBCO/PTO (epitaxial)	69	237	60	70	135 (?)	120 (?)	435
Voigt average (from crystal data)	*68*	*202*	*202*	*66*	*68*	*66*	
Reuss average (from crystal data)	*41.5*	*114*	*114*	*31*	*41.5*	*31*	
Sol–gel (random)	37	104	104	30	37	30	>490

values are nearly identical to those calculated from the elastic constants of cubic bulk platinum ($C_{11} = 347$ GPa, $C_{12} = 251$ GPa and $C_{44} = 76.5$ GPa) assuming a random orientation in the film and using a Voigt average (average of the elastic stiffness constants under random orientation). However, we point out that in the case of Pt the Reuss average (average of the elastic compliance constants under random orientation) leads to similar values ($C_{11} = 366$ GPa, $C_{44} = 62.5$ GPa) and, due to the experimental uncertainty related to the film thickness, also leads to a satisfactory fit with the recorded spectra.

An analysis of the elastic and piezo-electric properties of PTO single crystals studied by Brillouin scattering has been performed by Kalinichev *et al* [10]. These authors confirmed the previously measured [9] large tetragonal anisotropy of the elastic constants C^E at constant electric field ($C^E_{33} = 60$ GPa compared to $C^E_{11} = 237$ GPa; $C^E_{44} = 69$ GPa compared to $C^E_{66} = 104$ GPa) and the strong influence of the piezo-electric terms upon the velocities of

the propagating electro-acoustic waves. Note that the tetragonal anisotropy of the elastic tensor at constant electric induction (C^D), which is renormalized by the piezo-electric terms, is significantly reduced [9, 10] ($C_{33}^D = 145$ GPa; $C_{44}^D = 90$ GPa). Note also that, while C_{33}^D is easily accessible from the Brillouin scattering spectra of single crystals (it is directly related to the velocity of a longitudinal bulk mode propagating along the c-axis), C_{33}^E can be determined only less directly by a set of measurements in several suitable propagation directions. Thus its determination suffers from a larger experimental uncertainty [10].

In samples where the piezo-electric contribution vanishes due to spatial averaging over grains and domains with different orientations, the surface mode characteristics are expected to differ markedly from those obtained in single crystals. Namely, the propagation velocities of such modes will depend on the C^E constants only. Consequently they can provide an independent check of the unusually low value of C_{33}^E.

In order to account for our results on the PTO sol–gel polycrystalline thin films we used the fact that for our studied unpoled samples the random orientation will cancel out any piezo-electric contribution. We have compared our measured spectra to those that we have calculated by averaging the C^E tensor components reported in [10]. Due to the large tetragonal anisotropy, the Reuss and Voigt averages (see above) provide very different effective elastic constants: $C_{11} = 114$ GPa and $C_{44} = 41.5$ GPa for the Reuss, compared to $C_{11} = 202$ GPa and $C_{44} = 68$ GPa for the Voigt. We obtain a good fit to our data assuming the Reuss average, which gives rise to a strong effective softening of all the elastic constants, in agreement with our analysis of the spectra. The fit can be slightly refined through a small additional softening: the best results (see table 1) are obtained for $C_{11} = 104$ GPa and $C_{44} = 37$ GPa.

More or less pronounced differences between the shear elastic constants measured in thin films and those calculated from the bulk crystal data are commonly observed [17, 19, 22]. A softening of stiffnesses in thin films is most frequently reported; however, a hardening of a shear stiffness is sometimes observed [19]. These effects are related to the breakdown of the elastic properties in interfacial layers and in grain boundaries and to internal macroscopic and microscopic stresses [23]. They depend upon the thickness and upon the granularity of the films but, to our knowledge, a quantitative interpretation is still lacking.

One can easily verify that the large softening calculated for the Reuss set of averaged elastic constants is mainly due to the unusually small value of C_{33}^E. We point out that the averaged determinations are rather sensitive to C_{33}^E: a 10% change in C_{33}^E results in a 12.5% variation in the calculated C_{11} and C_{44}. Changes in the other C^E do not induce such drastic variations of the averaged tensor. Our results thus clearly confirm the very small value of C_{33}^E in PTO.

The comparison of the calculated and the experimental spectra is shown in figures 2 and 3. The optical transparency of PTO leads to rather complex spectra because the ripple contributions of the vacuum–PTO and of the PTO–Pt interfaces are of the same order of magnitude. One thus simultaneously observes a Rayleigh surface mode (ripple scattering on the free surface), a line corresponding to a Sezawa guided mode in the platinum sublayer (ripple scattering at the PTO–Pt interface), and an intense Sezawa guided mode within the PTO/Pt bilayer (constructive interference of both ripple contributions). In addition, the elasto-optic contribution is rather large and, as a consequence, we observe a complex feature related to a longitudinal resonance in the p–p spectra. Since the sub-structure of this feature cannot be experimentally resolved for the majority of the recorded spectra, we have plotted the mean velocity of the broad spectral line in figure 3. Finally, the elasto-optic scattering gives rise to a Love mode in the p–s spectra: in most of the previously reported Brillouin studies of thin films this mode could not be observed.

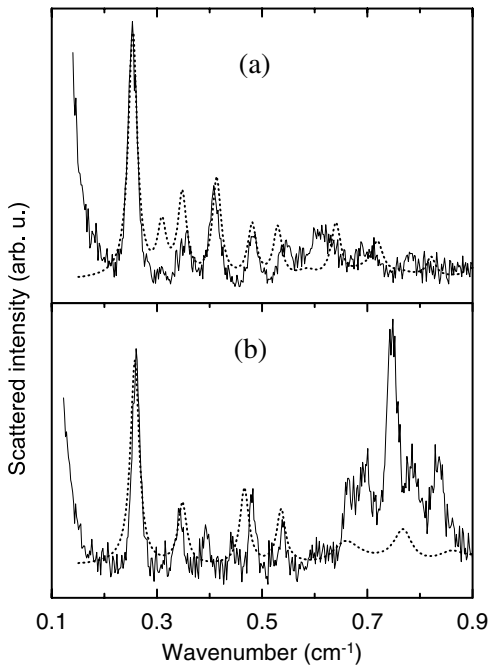

Figure 4. Epitaxial ablated samples: Brillouin spectra. (a) PTO/YBCO/STO; (b) PTO/STO. Angle of incidence: 60°. In-plane orientation: $q_{\parallel}$ parallel to a fourfold axis. Full curves: experimental data. Dotted curves: calculated spectra.

5.2. Films elaborated by laser ablation

The epitaxial nature of these films leads to significantly different Brillouin spectra compared to the sol–gel samples. Some typical examples are shown in figures 4(a) (PTO/YBCO/STO) and (b) (PTO/STO). Variations of surface velocities versus $q_{\parallel}h$ and versus the in-plane angle of propagation φ are reported in figures 5(a) and (b), respectively. The in-plane tetragonal anisotropy is clearly apparent, as seen in figure 5(b). The above mentioned large softening related to the random orientation of sol–gel films is not observed in the case of samples prepared by laser ablation.

The quantitative analysis was performed using the known values of the elastic constants of bulk STO. For the samples with a YBCO interlayer, we used the values of C_{ij} derived in our recent publication [19] concerning Brillouin scattering in the YBCO thin films ($C_{11} = 200$ GPa; $C_{55} = 44.5$ GPa; $C_{33} = 160$ GPa; $C_{13} = 80$ GPa; $C_{12} + 2C_{66} = 260$ GPa). Typical experimental spectra along with the fits are shown in figure 4 for both samples. These fits represent the calculated cumulative contribution of ripple and elasto-optic processes: they are characterized by the constants C_{11}, C_{33}, C_{55} and C_{13} at fixed electric field of bulk PTO (reported in [10]) and by the vanishing of piezo-electric terms. The absence of the piezo-electric contribution is supported by the hypothesis of a random distribution of $\pm\boldsymbol{c}$ ferroelectric domains in spite of the epitaxial character of the PTO film: the departure from such a distribution generally requires a poling through an applied electric field, but it can also arise from the presence of a conducting substrate, as recently observed in $PbZr_{0.2}Ti_{0.8}$ films [24]. However, we did not find evidence of a significant preferential polarization of the domains. To obtain an acceptable fit on the basis of a single ferroelectric domain, one would have to assume a very

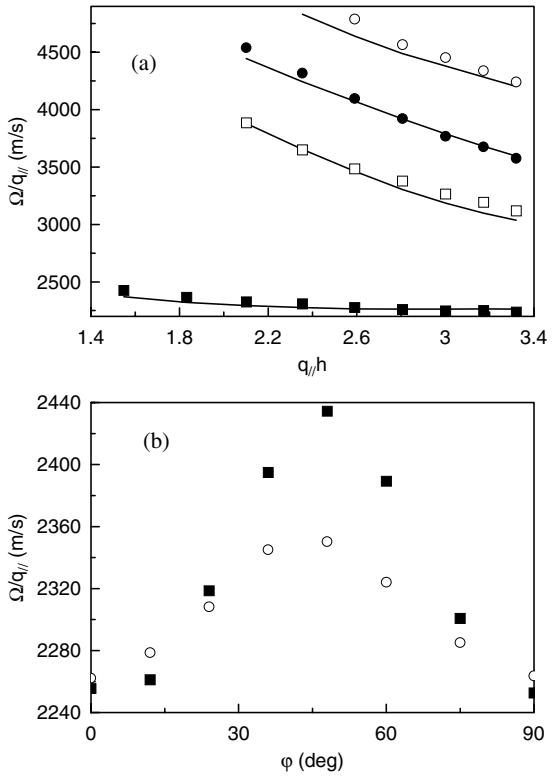

Figure 5. Epitaxial ablated PTO/YBCO/STO sample. (a) Variation of surface velocities ($\Omega/q_{\parallel}$) versus $q_{\parallel}h$ (h is the thickness of the PTO film). Experimental, points; calculations, curves. (b) Variation of surface velocities versus in-plane angle φ (0° and 90° correspond to the propagation along $\boldsymbol{a}$ and $\boldsymbol{b}$ axes): (■) experiment; (○) calculation.

large softening of C_{55} (by more than 30%). In contrast, the model of a random distribution of $\pm\boldsymbol{c}$ domains accounts for the spectra without any renormalization of the bulk elastic constants. We thus believe that (i) the absence of a piezo-electric contribution is experimentally confirmed, and that (ii) in contrast with the case of sol–gel samples, the grain boundaries do not significantly affect the effective elastic constants.

The measured spectra depend significantly upon the presence of a YBCO interlayer. The number and the positions of the spectral lines related to the guided modes differ and, in addition, the spectra of the PTO/STO sample (figure 4(b)) show an intense broad line between 0.65 and 0.85 cm^{-1}. The position of this line does not depend on the angle of incidence and corresponds to a quasi-transverse bulk mode of PTO. The large full width at half maximum (FWHM) of this line is due to the uncertainty of the wavevector q of the bulk mode related to the finite PTO film thickness h and is in agreement with the relation $\Delta q \approx 1/h$. This phenomenon illustrates again the high efficiency of the elasto-optic process in PTO. On the other hand, our model is not able to explain why the bulk mode is detected in the PTO/STO structure while it is absent in the PTO/YBCO/STO sample.

In spite of the above-described general satisfactory agreement between expected and measured data, some points are not yet completely clear. First, we cannot perfectly reproduce the relative intensities of the observed lines: in figure 4(a), for instance, the second observed Brillouin line is very weak while its calculated intensity is rather large. Other slight discrepancies can be found in figure 4(b). However, the relative intensities are very sensitive

to many parameters which cannot be precisely determined; a better fit could probably be obtained, but, in our opinion, such an improvement would not really advance the qualitative interpretation of the spectra.

Finally, the experimentally observed in-plane anisotropy, as shown in figure 5(b), is significantly larger than that expected from our calculations using the bulk elastic constants [10]. Our detailed analysis shows that the velocities of the surface waves propagating along the a axis depend only upon C_{11}, C_{33}, C_{13} and C_{55}, while for an arbitrary direction of propagation in the $(\boldsymbol{a}, \boldsymbol{b})$ plane they will also depend upon $(C_{12} + 2C_{66})$. In principle, it is possible to adjust $(C_{12} + 2C_{66})$ in order to account for the large observed anisotropy. However, this procedure leads to a strong renormalization of $(C_{12} + 2C_{66})$—to a hardening of about 30%—which does not seem credible in view of the above-mentioned good agreement of our spectra with the elastic constants of the bulk crystal for the propagation along the $\boldsymbol{a}$ crystallographic axis.

6. Variations versus temperature: the ferroelectric–paraelectric transition

The ferroelectric–paraelectric phase transition is expected to induce large variations in the Brillouin spectra since in the tetragonal $4mm$ ferroelectric phase C_{33} and C_{66} strongly differ from C_{11} and C_{44}, respectively, while in the paraelectric $m3m$ cubic phase one necessarily has $C_{33} = C_{11}$ and $C_{66} = C_{44}$. In a bulk PTO crystal, where the phase transition occurs at $T_C = 490\,^{\circ}\mathrm{C}$, the variations of some Brillouin spectra versus temperature have been studied [9]. The authors observe that C_{66} does not show a significant variation versus temperature and that, consequently, C_{44} suffers a large hardening at the phase transition. As to the longitudinal constants, a moderate softening of C_{11} was observed at T_C, which implies a large increase of C_{33}.

It is known that in PTO thin films the transition temperature strongly depends upon the crystal texture and upon the underlying substrate. These temperature variations are generally interpreted as arising from internal stresses in the films which couple with the electric polarization vector of the ferroelectric [6]. In addition, ferroelectric domains of small dimensions induce a lowering of T_C [25–27]. In the case of the sol–gel films, from our measurements of the linear dimensions of the grains, we expect that the majority of them consist of single ferroelectric domains [28] which, according to [26, 27], are too large (more than 100 nm) to modify T_C significantly. The grains of the epitaxial films presumably show a polydomain structure due to their larger linear dimensions (200–250 nm); however, the domain size (around 50 nm: see [28]) is not expected to induce a decrease of T_C by more than 10 °C [27].

The Brillouin spectra of the sol–gel films do not show frequency variation up to about 480 °C. The frequency variation of the Love mode versus temperature is reported in figure 6 and it indicates an increase of the transition temperature compared to the bulk. Due to experimental limitations, it is not possible to precisely evaluate T_C. However, our results seem in agreement with the 40 °C increase determined from a Raman study on very similar samples by Fu *et al* [7].

The results concerning the pseudo-Rayleigh line for a PTO/STO film are reported in figure 7(a) which shows the variation of the derived velocity and of the FWHM versus temperature. The FWHM presents a very sharp and well defined maximum which is assumed to correspond to the phase transition. We see that there is an increase in T_C of 40 °C. The occurrence of an increase in T_C agrees with recent results deduced from x-ray diffraction and Raman spectroscopy on PTO films grown on MgO substrates buffered with a layer of STO [29]: they are interpreted in terms of two-dimensional compressive stresses in the PTO films deriving from the mismatch between the lattice parameter of the STO substrate and of the PTO film as well as from the thermal expansivity of the film and substrate.

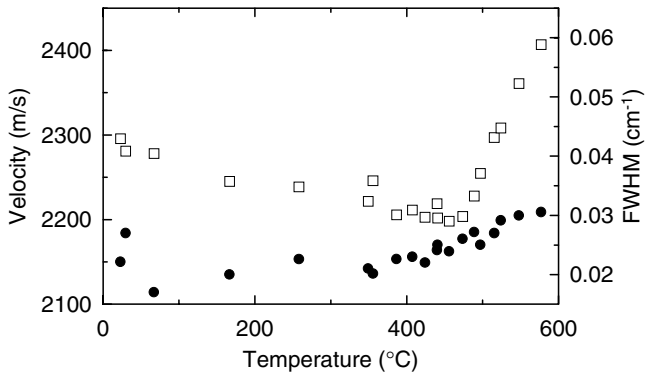

Figure 6. Sol–gel sample: variation of (□) propagation velocity and (●) damping (FWHM) versus temperature for the Love mode.

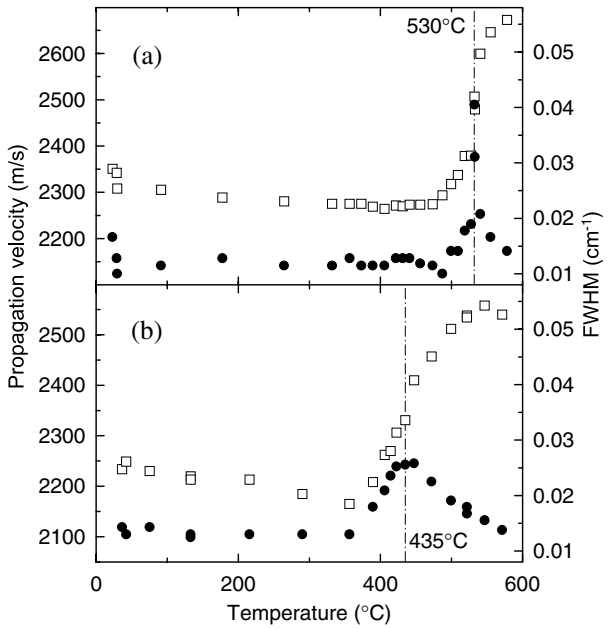

Figure 7. Epitaxial ablated samples: variation of (□) propagation velocity and (●) damping (FWHM) versus temperature for the pseudo-Rayleigh mode. (a) PTO/STO, (b) PTO/YBCO/STO.

The increase of the velocity from below to above the transition is connected to the hardening by a factor of 1.4 of an 'effective' elastic constant. This enhancement can be compared to the ratio $C_{44}/C_{66} = 1.5$ reported in the ferroelectric phase at room temperature; this suggests that the frequency shift of the pseudo-Rayleigh line is mainly due to the variation of the shear elastic constant C_{44}: in the cubic paraelectric phase C_{44} does not differ from C_{66} which, in the bulk crystal, seems to be independent of the temperature [9].

The results concerning the pseudo-Rayleigh line for a PTO/YBCO/STO film are reported in figure 7(b). The phase transition is also clearly apparent. The velocity increase is nearly the same as in the PTO/STO film and the position of the maximum of the FWHM allows us to make a fairly precise determination of T_C. In contrast with the PTO/STO film we observe a downshift

in T_C, which now occurs at 435 °C. This 55 °C decrease compared to the bulk PTO value would argue for the presence of extensive two-dimensional stresses in the PTO film. However, this conclusion is subject to controversy since recent theoretical approaches [30] predict an increase in T_C regardless of the sign of the stresses (compressive or extensive). There are two facts to consider with respect to the YBCO buffer layer. These are that, as mentioned above, (1) the in-plane lattice parameters of YBCO are less than that of the PTO, whereas the in-plane lattice parameter of the STO substrate is larger than that of PTO, and (2) the YBCO undergoes a tetragonal to orthorhombic transition anywhere between 400 and 700 °C depending on the oxygen partial pressure. As to point (2) such a change in YBCO at a temperature below the T_C of bulk PTO could provoke a ferroelectric phase transition and, consequently, a change in the elastic constants of the adjacent PTO film. Of course this is only speculative. Theoretical treatments of the subject consider ferroelectric PTO layers in direct contact with the single-crystal substrate. The analysis becomes necessarily more complex when intermediate layers are introduced. In addition the thermal expansivity of the substrates and of the films must be taken into account as well as the lattice mismatch when considering stresses in thin films. Finally the film thickness is a not unimportant parameter that should be taken into account. In brief, there is no evident justification of the inversion of the sign of the stress when a YBCO buffer is introduced. In any case we do envisage performing x-ray measurements as a function of temperature to see in what temperature range the YBCO orthorhombic to tetragonal transition is taking place, and also to compare our Brillouin determined T_C with that determined by x-ray diffraction.

7. Conclusion

We have presented Brillouin scattering results on polycrystalline and epitaxial PTO thin films as a function of temperature. The model that we have developed to treat the response of these layered heterostructures explains most of the data in a satisfactory fashion and provides us with a means to apply the Brillouin technique to other ferroelectric materials.

Acknowledgments

The authors thank B Malic from the J Stefan Institute of Ljubiana (Slovenia) for providing the sol–gel samples. This work was partly supported by the Ministry of Education of the Czech Republic (project No LN00A032).

References

[1] Ghosex P and Rabe K M 2000 *Appl. Phys. Lett.* **76** 2767
[2] Tybell T, Ahn C and Triscone J M 1999 *Appl. Phys. Lett.* **75** 856
[3] Rossetti G A Jr, Cross L E and Kushida K 1991 *Appl. Phys. Lett.* **59** 2524
[4] Yamamoto T and Matsuoka H 1994 *Japan. J. Appl. Phys.* **33** 5317
[5] Sun L, Chen Y-F, He L, Ge C-Z, Ding D-S, Yu T, Zhang M-S and Min N-B 1997 *Phys. Rev.* B **55** 12218 and references therein
[6] Yuzyuk Yu I, Farhi R, Lorman V L, Rabkin L M, Sapozhnikov L A, Sviridov E V and Zakharchenko I N 1998 *J. Appl. Phys.* **84** 452
[7] Fu D S, Iwasaki H, Suzuki H and Ishikawa K 2000 *J. Phys.: Condens. Matter* **12** 399
[8] Burns G and Scott B A 1972 *Phys. Rev.* B **7** 3088
[9] Li Z, Grimditch M, Foster C M and Chan S-K 1996 *J. Phys. Chem. Solids* **57** 1433
[10] Kalinichev A G, Bass J D, Sun B N and Payne D A 1997 *J. Mater. Res.* **12** 2623
[11] Loudon R 1978 *Phys. Rev. Lett.* **40** 581
[12] Loudon R and Sandercock J R 1980 *J. Phys. C: Solid State Phys.* **13** 2609

[13] Albuquerque E L 1980 *J. Phys. C: Solid State Phys.* **13** 2623
[14] Albuquerque E L, Loudon R and Tilley D R 1980 *J. Phys. C: Solid State Phys.* **13** 1775
[15] Velasco V R and Garcia-Moliner F 1980 *J. Phys. C: Solid State Phys.* **13** 2237
[16] Velasco V R and Garcia-Moliner F 1980 *Solid State Commun.* **33** 1
[17] Djemia P 1998 *PhD Thesis* Université Paris-Nord, France
[18] Farnell G W 1970 Properties of elastic surface waves *Physical Acoustics* vol 6, ed W P Mason and R N Thurston (New York: Academic) p 109
[19] Kuzel P, Dugautier C and Moch P 2001 *J. Phys.: Condens. Matter* **13** 167
[20] Camley R E and Nizzoli F 1985 *J. Phys. C: Solid State Phys.* **18** 4795
[21] Karkut M G, Le Marrec F, Marechal C, Steinseth R K, El Marssi M, Farhi R, Dellis J L and Portemer F 1999 *Ferroelectrics* **225** 1067
[22] Subramanian S, Sooryakumar R, Prinz G A, Jonker B T and Idzerda Y U 1994 *Phys. Rev.* B **49** 17319
[23] Schäfer J D, Näfe H and Aldinger F 1999 *J. Appl. Phys.* **85** 8023
[24] Ganpule C S, Nagarajan V, Hill B K, Roytburd A L, Williams E D, Ramesh R, Alpay S P, Roelofs A, Waser R and Eng L M 2002 *J. Appl. Phys.* **91** 1477
[25] Shih W Y, Shih W-H and Aksay I A 1994 *Phys. Rev.* B **50** 15575
[26] Ishikawa K, Yoshikawa K and Okada N 1988 *Phys. Rev.* B **37** 5852
[27] Zhong W L, Jiang B, Zhang P L, Ma J M, Cheng H M, Yang Z H and Li L X 1993 *J. Phys.: Condens. Matter* **5** 2619
[28] Ren S B, Liu C J, Liu J S, Shen H M and Wang Y N 1996 *Phys. Rev.* B **54** 14337
[29] Le Marrec F, Farhi R, Dkhil B, Chevreul J and Karkut M G 2001 *J. Eur. Ceram. Soc.* **21** 1615
[30] Pertsev N A, Zembiligotov N A and Tagantsev A K 1998 *Phys. Rev. Lett.* **80** 1988